Analytical Calculation of Yoke Flux Patterns in Fractional-Slot Permanent Magnet Machines

Astrid Røkke and Robert Nilssen

Department of Electric Power Engineering, Norwegian University of Science and Technology, 7491 Trondheim, Norway

Machine design problems are often solved under the assumption of no-load when calculating iron flux densities. However, it is particularly important to account for the fluxes from the stator currents, the armature reaction, in fractional-slot machines. The fluxes from the permanent magnets and the armature reaction both vary in time with the electrical frequency. By studying the flux that flows along the stator yoke behind every slot in such a machine, it is revealed that the armature reaction flux does not have the same amplitude behind all slots. In addition, it is revealed that the time-varying no-load and armature reaction fluxes are shifted in time, with different phase shifts behind different slots. The sum of the no-load and armature reaction fluxes, namely, the load flux, depends on both the amplitudes of the fluxes and the phase shift between them. The resulting load flux behind each slot varies significantly. In four investigated machines, the ratio of the highest to the lowest load flux amplitude ranges between 1.6 and 6. The load flux can be significantly higher than the no-load flux. The flux calculations are verified through finite-element analysis in all four machines, and the error in the maximum load flux ranges between 2% and 6%.

Index Terms— **Armature reaction, fractional-slot machines, permanent magnet (PM) machines, stator flux patterns.**

I. Introduction

A. Iron Yoke Flux Prediction

THE magnetic fluxes in the stator and rotor yokes of permanent magnet (PM) machines have two sources: the magnetic fields created by the PMs and the magnetic fields created by the current in the stator windings, namely, the armature reaction. Both of these sources create fields that vary with both time and space. The time variation is caused by the rotation of the rotor and the time variation of the current in the windings. These fluxes both vary with the electrical frequency, as determined by the rotational speed and the number of magnetic poles. However, they are not in phase, at least not in all parts of the yokes. This paper will show how the PM flux and the armature reaction flux together create flux patterns with considerable spatial variations. This phenomenon has not, to the best of our knowledge, been reported before in the literature.

The magnetic flux densities in iron yokes are calculated in a variety of ways and for various reasons. The most common reasons are to determine iron losses and to prevent iron saturation. In many cases, only the no-load flux is calculated, and the armature reaction is disregarded [1], [2]. PM machines are typically designed, such that the air-gap flux density caused by the armature reaction is lower than the air-gap flux from the magnets. This will prevent the demagnetization of the PMs in the case of fault currents in the stator windings. However, it does not necessarily ensure that the *yoke* flux densities originating from the armature reaction remain low. In non-overlapping concentrated-coil machines with significant subharmonics, the stator and rotor yoke fluxes can be much higher than the air-gap flux. This can cause the back iron to be heavily saturated, and in such a case, the magnetic flux can spread into nearby conductive materials, thereby inducing losses.

With an increasing focus on design optimization, it is also important to include the armature reaction flux in magnetic models. In [3], all geometric parameters except the air-gap length are free variables, in addition to the current density. The design is limited by constraints on the efficiency, power factor, and the flux densities in the stator and rotor yokes and the stator teeth. If these constraints are imposed only on the no-load flux density, then the resulting optimal design may be heavily saturated at full load. To avoid optimization models that yield unfeasible designs, suitable constraints must be included. Thus, the calculations of the armature reaction flux density must be performed.

The most accurate method of performing such calculations is finite-element analysis (FEA). To be able to see the flux patterns, one will have to record the flux as a function of time behind all slots. In some cases, however, FEA is not practical. Designers might not have access to or competence enough to use the softwares, or the calculations may be part of an optimization process, which would become unnecessary slow if an FEA simulation was to be included. In this paper, a simple method using only two lumped parameter models (LPMs) is used to estimate the fluxes through all parts of the stator and rotor yokes and teeth.

The objects of study are the yoke and teeth fluxes, not the flux densities. The flux at position 1, for example, is the integral of the tangential flux density over the line connecting slot number one with the outer periphery (Fig. 3). To limit the scope of this paper, attention is focused on the stator yoke fluxes.

B. Literature

Little effort has been directed toward the calculation of the magnetic fluxes in PM machines caused by the armature reaction. In 1993, a paper [4] was written on the instantaneous prediction of the air-gap and magnet fluxes caused by the

Manuscript received February 18, 2016; revised August 23, 2016; accepted October 17, 2016. Date of publication November 2, 2016; date of current version March 16, 2017. Corresponding author: A. Røkke (e-mail: astrid.roekke@ntnu.no).

Color versions of one or more of the figures in this paper are available online at http://ieeexplore.ieee.org.

Digital Object Identifier 10.1109/TMAG.2016.2623583

armature reaction, including all harmonic content. Only the air-gap and magnet regions, not the stator yokes, were included in the calculations.

In the last decade, focus has been placed on the rotor losses caused by subharmonic magnetic fluxes in fractional-slot machines with concentrated windings [5]–[7], and methods have been developed to determine the rotor fluxes in such machines. One analytical technique for this purpose is presented in [8] and is capable of predicting the on-load flux density waveforms in different parts of the stators of PM machines. However, the technique is only applied to an integral-slot machine, and focus is placed on the flux density waveforms in different parts of a tooth.

In [9], the stator flux and iron losses of a non-overlapping concentrated winding machine are investigated, but the stator yoke flux is measured at only one point, and the spatial harmonic pattern of the stator yoke is not studied.

The flux patterns in stators with fractional-slot non-overlapping windings are briefly mentioned in [10]. It is suggested that in double-layer wound machines, in which adjacent teeth are wound with coils of the same phase but opposite polarity, some portions of the stator yoke can be reduced, because some parts are less used by the flux than others. Only armature reaction fluxes are considered. In this paper, it is shown that when the no-load and armature reaction fluxes are combined, single-layer wound machines can exhibit even larger variations in their flux load distributions.

In [11] and [12], the stator core flux density is investigated for an interior magnet machine with concentrated coils. It is claimed that the investigated machine possesses electric and magnetic symmetry, which causes the yoke flux behind each slot to exhibit identical patterns, only separated in time. In sections II and III, it will be shown that for three-phase fractional-slot machines with three slots per pole, the magnetic symmetry is indeed, such that the yoke flux is identical behind each slot.

C. Hypothesis

LPMs are easy to establish and quick to solve. No-load fluxes are often determined using LPMs. Armature reaction fluxes can also be found using this method. Combining the results of these two calculations, however, is not straightforward. In different parts of the machine, the no-load fluxes will either sum with or be subtracted from the armature reaction fluxes. By studying the flux patterns of four different fractional-slot machines with single and double layers and with concentrated and distributed windings, a method for combining the no-load and armature reaction fluxes will be presented.

The proposed method is expected to be particularly useful for preliminary designs and for optimization studies in which FEA is not applied. For exact estimates of the flux densities and iron losses, FEA can be used.

II. Methodology

A. Lumped Parameter No-Load Magnetic Circuit

The electromagnetic model for predicting the no-load magnetic fluxes is based on the lumped parameter network shown in Fig. 1 [13]. R_s and R_r are the stator and rotor yoke reluctances, respectively. Both are set to zero because of the high relative permeability of iron. R_g is the air-gap reluctance, R_{ml} is the magnet-to-magnet leakage reluctance, R_{mr} is the magnet-to-rotor-yoke leakage reluctance, R_{pm} is the magnet reluctance, and ϕ_{pm} is the remanent flux of the PM. The physical air gap is multiplied by a Carter coefficient to account for the variation of the flux density in the air gap caused by slotting. From the magnetic circuit, one can find that the amplitude of the air-gap flux is

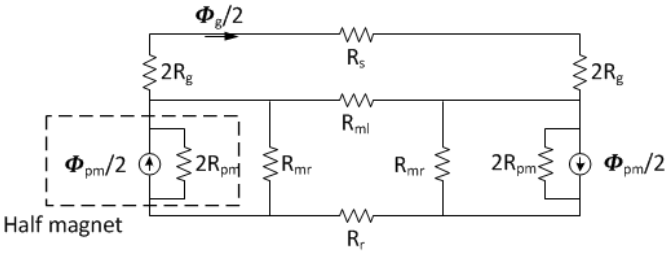

Fig. 1. No-load magnetic circuit.

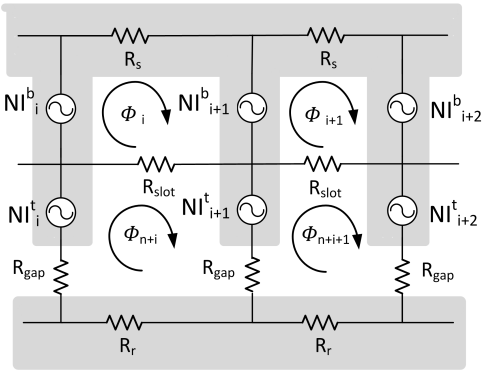

Fig. 2. Armature reaction magnetic circuit.

$$\phi_g = \frac{R_{\mathrm{ml}} R_{\mathrm{pm1}} \phi_{\mathrm{pm}}}{2(R_g R_{\mathrm{ml}} + 2R_g R_{\mathrm{pm1}} + R_{\mathrm{ml}} R_{\mathrm{pm1}}/2)} \tag{1}$$

where R_{pm1} is the reluctance resulting from $2R_{\mathrm{pm}}$ and R_{mr} in parallel. The amplitude of the no-load flux in the stator yoke is $\phi_g/2$. The no-load flux has a spatial distribution, and the phase shift between slots is

$$\alpha_s = 2\pi \frac{p}{Q} \tag{2}$$

where p is the number of pole pairs and Q is the number of slots.

The no-load calculation is time-stepped. The flux at position 1 is at a maximum at $t = 0$, and the fluxes at the remaining positions lag behind in accordance with their phase angles. The fluxes in all teeth and behind every stator slot are found for each time step. For simplicity, it is assumed that the flux is sinusoidally varying in time.

B. Lumped Parameter Armature Reaction Circuit

The magnetic circuit shown in Fig. 2 is used to find the magnetic flux densities in the teeth and yokes due to the

armature reaction. R_{gap} is the reluctance of the magnet and the air gap combined, R_{slot} is the slot leakage reluctance, N is the number of turns per coil, I is the current, and ϕ is the mesh flux. The subscript i indicates the slot number, b denotes the bottom layer, and t denotes the top layer of the winding in the case of two-layer windings. When the winding is of the single-layer type or the double-layer winding is of the concentrated type, $\text{NI}_i^b = \text{NI}_i^t$. The figure shows only a part of the mesh network.

A large machine can often be split up into multiple sections that are exact copies, each of which includes one base winding. n is the number of slots per base winding, and n teeth must be included in the circuit.

In a slot that contains stator coils in which the current is distributed evenly and linearly, the stored magnetic energy is $1/3$ of the magnetic energy that would be present if the current were concentrated at one point in the bottom of the slot [14]. This should be considered when modeling the slot leakage reluctance. As a simplification, the slot leakage reluctance can be calculated using the equation

$$R_{\text{slot}} = L\frac{3w_{\text{slot}}}{\mu_0 d_{\text{slot}}} \tag{3}$$

where L is the active length, w_{slot} is the slot width, μ_0 is the relative permeability of air, and d_{slot} is the slot depth.

The LPM contains three nodes per tooth. This is a coarse division and can be refined to obtain more precise estimates of the flux densities. For machines with salient poles, more nodes should be added at the slot opening. With the aid of Fig. 2, one can write the following equations:

$$\begin{aligned}&\text{NI}_{i+1}^b + \phi_{i+1}R_s - \text{NI}_{i+2}^b \\ &\quad + (\phi_{i+1} - \phi_{n+i+1})R_{\text{slot}} = 0\end{aligned} \tag{4}$$

$$\begin{aligned}&(\phi_{n+i+1} - \phi_{n+i})R_{\text{gap}} + \text{NI}_{i+1}^t \\ &\quad + (\phi_{n+i+1} - \phi_{i+1})R_{\text{slot}} - \text{NI}_{i+2}^t \\ &\quad + (\phi_{n+i+1} - \phi_{n+i+2})R_{\text{gap}} + \phi_{n+i+1}R_r = 0\end{aligned} \tag{5}$$

A set of $2n$ equations forms a matrix equation of the form

$$\text{NI} = \phi R \tag{6}$$

where R is a $2n \times 2n$ matrix and NI and ϕ are vectors with a length of $2n$. The first half of ϕ contains the fluxes in the stator back yokes, and the second half contains the fluxes in the rotor back yokes. The tooth fluxes at the top and bottom are $\phi_{i+1} - \phi_i$ and $\phi_{n+i+1} - \phi_{n+i}$, respectively.

The armature reaction flux calculation is also time-stepped, and the fluxes are found at all positions for all time steps. The phase currents are

$$\begin{aligned}I_R &= \widehat{I}\cos(\omega(t - t_0)) \\ I_S &= \widehat{I}\cos(\omega(t - t_0) + 2\pi/3) \\ I_T &= \widehat{I}\cos(\omega(t - t_0) - 2\pi/3).\end{aligned} \tag{7}$$

1) Load Angle: For the maximum torque production per unit of current, the current must be on the q-axis and in phase with the no-load voltage. To find the correct load angle, the no-load fluxes found in Section II-A is summed up for all slots composing phase R as a function of time. The induced voltage in phase R is $V_R = -d\phi/dt$. t_0 is set equal to the time when the induced R-phase voltage peaks. This places the current in the q-axis.

TABLE I
INVESTIGATED MACHINES

Machine	A	B	C	D
Number of poles	110	110	40	40
Number of slots	120	120	168	168
Winding layers	1	2	1	2
Winding type	conc	conc	distr	distr
Magnet thickness	16 mm	16 mm	16 mm	16 mm
Magnet width	80 mm	80 mm	180 mm	180 mm
Slot depth	73 mm	73 mm	63 mm	63 mm
Slot width	32 mm	32 mm	25 mm	25 mm
Tooth width	51 mm	51 mm	34 mm	34 mm
Rotor yoke	57 mm	57 mm	80 mm	80 mm
Stator yoke	47 mm	47 mm	70 mm	70 mm

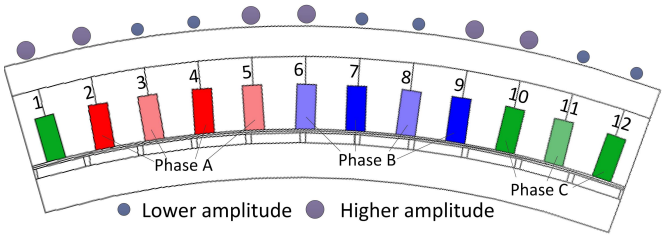

Fig. 3. Winding layout of one tenth of Machine A.

C. Investigated Machines

The influence of the armature reaction on the stator and rotor fluxes depends on the machine's topology and winding layout. Four different machines with fractional slots and different winding layouts are investigated in this paper. The major properties of the investigated machines are summarized in Table I.

Fig. 3 shows one tenth of the winding layout of Machine A, with single-layer concentrated coils.

III. RESULTS

A. No-Load Fluxes

The LPM with no-load is used to find the no-load fluxes. The fluxes in Machine A are illustrated here. Fig. 4 shows how the flux varies with time at different positions in Machine A. At $t = 0$, one PM is located directly below the tooth to the left of position 1. In Fig. 5, only the no-load fluxes at positions 6–9 of Machine A are shown. The flux is the same for all positions, and only shifted in time.

B. Armature Reaction

The LPM for the armature reaction is used to find the armature reaction fluxes. To illustrate the difference in magnitude between air-gap flux and yoke flux, Table II lists the tangential fluxes in the stator and rotor back yokes as well as the radial fluxes in the teeth taken at *one* instance. The position numbers refer to Fig. 3. It is clear that both the stator yoke and rotor yoke fluxes are significantly higher than the tooth fluxes.

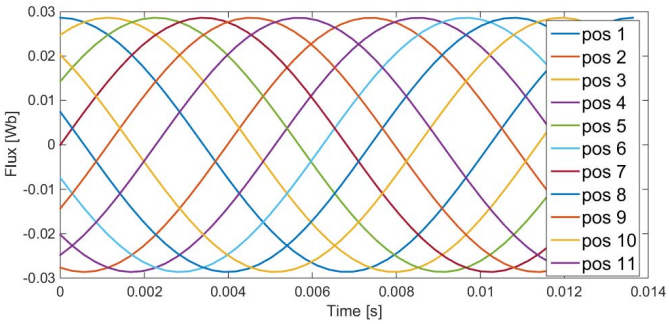

Fig. 4. No-load flux as a function of time in Machine A.

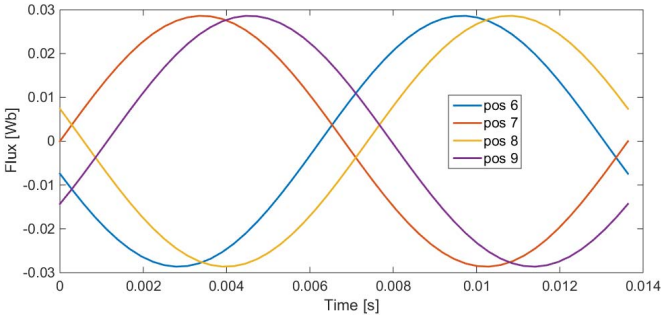

Fig. 5. No-load fluxes at positions 6–9 in Machine A.

TABLE II
STATIONARY ARMATURE REACTION FLUXES [mWb]

Position	Stator flux	Rotor flux	Air gap flux
1	25.4	-26.9	-13.1
2	30.7	-27.8	0.9
3	-2.7	-0.3	-27.5
4	4.3	-1.4	1.1
5	-29.0	26.1	-27.5
6	-23.7	25.2	1.0
7	-40.6	39.1	-14.0
8	-37.0	38.6	0.6
9	-54.5	53.0	-14.4
10	-54.4	53.0	0.0
11	-38.0	39.4	13.6
12	-41.3	39.9	-0.5

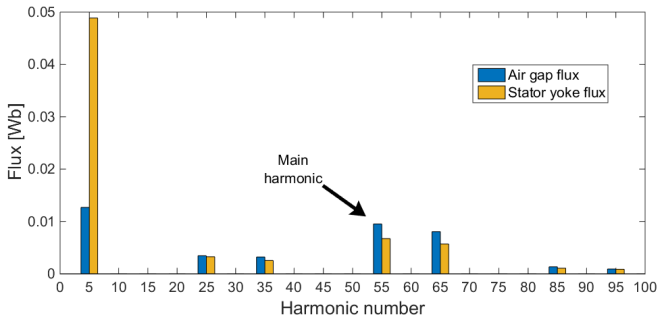

Fig. 6. Harmonic contents of the stator yoke and air-gap fluxes.

This is in contrast to the *no-load* operation for concentrated-coil machines, where the fluxes in the stator and rotor yokes are half of the flux in the teeth because half the tooth flux will go to the left and the other half will go to the right.

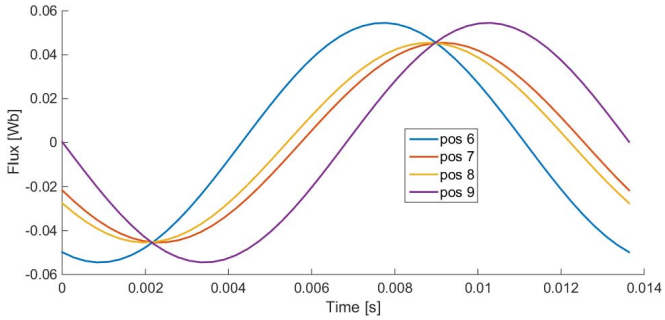

Fig. 7. Armature reaction fluxes at positions 6–9 in Machine A.

It is generally known that in a fractional-slot concentrated-coil machine, the air-gap flux often has high subharmonics [15], [1]. A Fourier analysis of the flux distributions presented in Table II for both the air-gap fluxes and stator yoke fluxes reveals that although the amplitudes of the air gap flux subharmonics are high, the amplitudes of the stator yoke flux subharmonics are even higher. The lowest harmonic (5th) is seven times higher than the main harmonic (55th), as shown in Fig. 6.

Above, the spatial distribution of the armature reaction flux is investigated. The armature reaction flux in the stator yoke is also studied as a function of time. The time variations of the fluxes at positions 6–9 in Machine A are shown in Fig. 7. The pattern of each of the four curves repeats itself for each of the three phase groups.

It has been shown that the *no-load* flux amplitude is equal at every position. However, the *armature reaction* flux amplitudes are not equal at all positions. In Machine A, the winding layout causes the fluxes on the outer sides of the phase group to be higher than those in the middle of the phase group. Although the armature reaction creates a flux pattern that rotates, this pattern is not evenly distributed along the stator. This is illustrated by the dark circles shown in Fig. 3. Such uneven patterns can also be observed in the three other machines (Fig. 8). Machines A and B possess 12 slots in an antisymmetric section, and Machines C and D possess 42 slots in a symmetric section. The biggest variation in stator yoke armature flux is found in Machine B.

When the three phases are distributed symmetrically within the section, the flux pattern is repeated three times in each section.

C. FEA Model

FEA can be used to verify the analytical results and to generate illustrations of the flux lines in the machines. FEA models of the four machines have been created in COMSOL. One tenth each of Machines A and B are modeled, and antisymmetry conditions are imposed on the side boundaries. One quarter each of Machines C and D are modeled, with symmetry conditions imposed on the side boundaries. The laminations have a nonlinear magnetization curve, as shown in Fig. 9.

First, a no-load calculation is performed under rotation. The fluxes through the different parts of the stator back yoke are recorded as a function of time. The flux density and flux

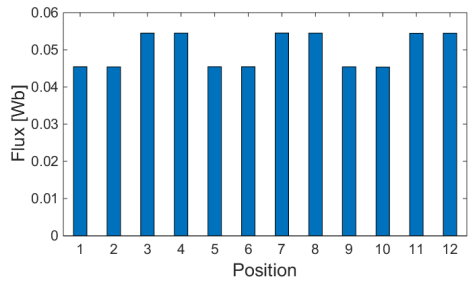

(a)

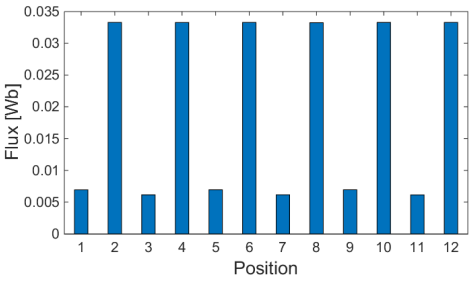

(b)

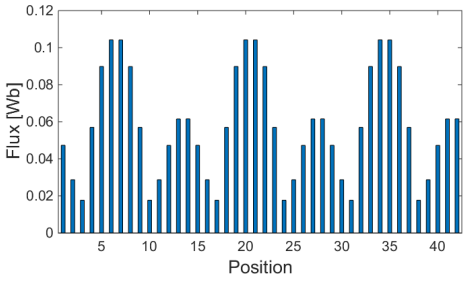

(c)

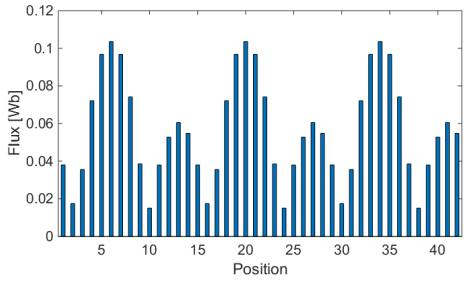

(d)

Fig. 8. Armature reaction flux amplitudes in Machines A–D. (a) Machine A. (b) Machine B. (c) Machine C. (d) Machine D.

lines of Machine A are shown in Fig. 10. The flux lines flow tangentially along the stator yoke in every other direction as the position of interest moves along the stator.

Second, an armature reaction calculation is performed with the current placed in the q-axis and the PMs deenergized. The resulting flux density and flux lines of Machine A are shown in Fig. 11. The fifth harmonic can be clearly seen.

Finally, superposition is assumed, and the time-varying flux from the no-load simulation is added to the time-varying flux from the armature reaction simulation at each time step. This makes it possible to find the no-load flux, the armature reaction

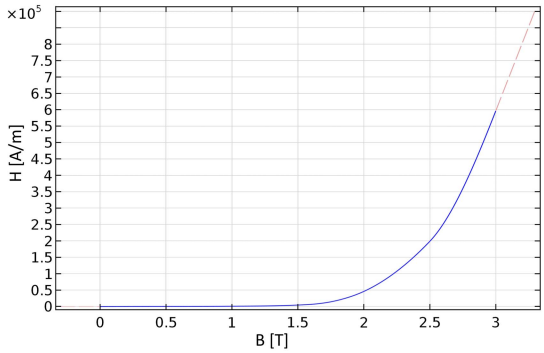

Fig. 9. Saturation curve of the soft magnetic material.

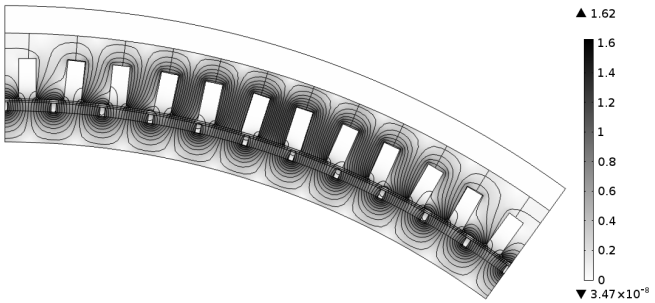

Fig. 10. No-load flux density [T] and flux lines.

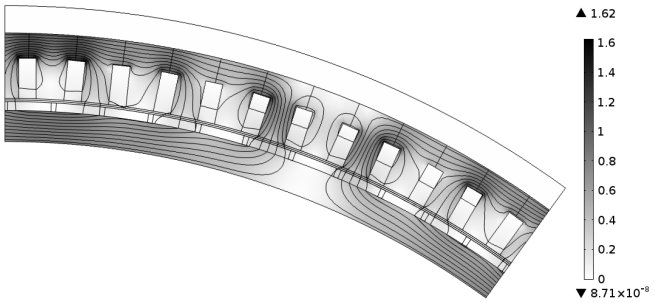

Fig. 11. Armature-reaction-induced flux density [T].

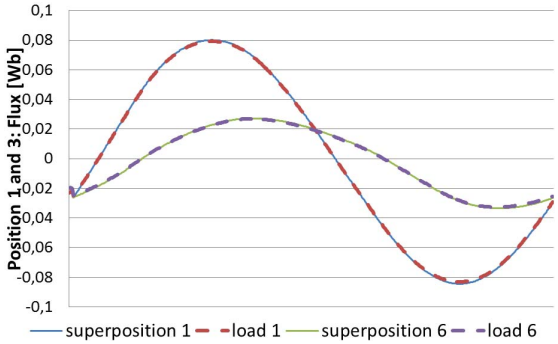

Fig. 12. Fluxes obtained via superposition compared with fluxes obtained under load.

flux and the load flux from only two time-stepped FEA simulations. It is assumed that the superposition of the two results is sufficient to predict the load flux. A simulation under load, with magnetized magnets and the armature reaction, is performed to verify this assumption. The fluxes in Machine A at positions 1 and 6 are shown in Fig. 12, showing that the assumption is valid. The error in the amplitude is less than 1%.

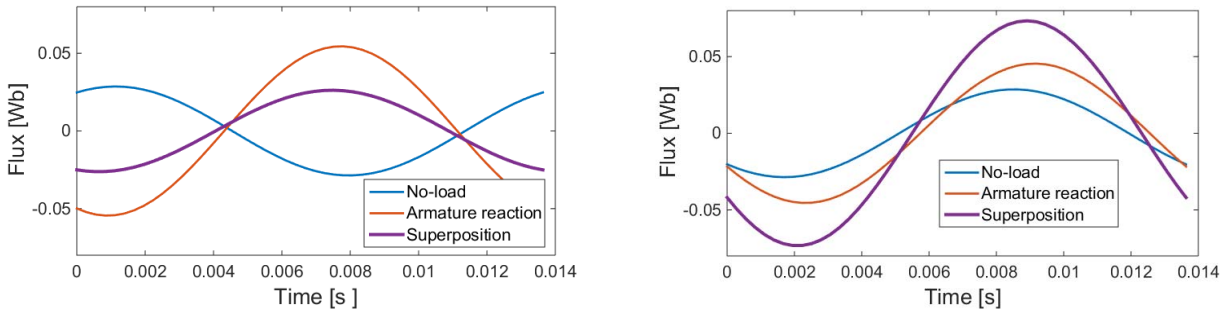

Fig. 13. No-load, armature reaction, and superposed fluxes as functions of time. (a) Position 6. (b) Position 7.

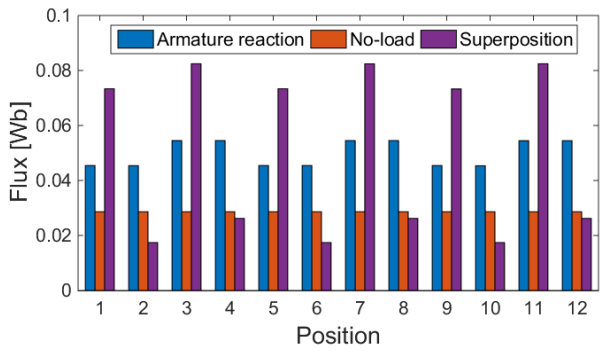

Fig. 14. Machine A: flux amplitudes in positions 1–12.

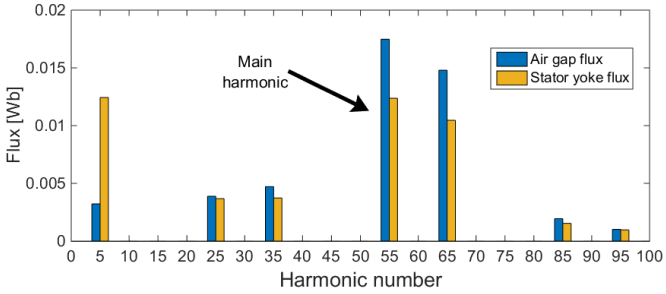

Fig. 15. Harmonic content in Machine B.

Further simulations have shown that, for the given material, the error of the assumption of superposition is less than 2% when the total mean flux density is less than 1.9 T.

D. No-Load and Armature Reaction Fluxes Combined

The results from the no-load LPM and the armature reaction LPM are combined at each time step, as in the FEA analysis. When the two flux patterns shown in Figs. 5 and 7 are combined, the no-load flux lines are alternately summed with or subtracted from the fifth harmonic at every other position. This is shown in Fig. 13, which shows how the armature reaction and no-load fluxes are combined to obtain the superposed fluxes at positions 6 and 7. At position 6, the armature reaction and no-load fluxes are nearly opposite in phase, whereas at position 7, they are nearly in phase.

Consequently, the magnitude of the load flux is more highly dependent on the phase difference between the no-load and armature reaction fluxes than on the amplitude of the armature reaction flux. Although the highest armature reaction flux amplitude is observed at position 6, the combined flux amplitude is much higher at position 7.

Fig. 14 shows the amplitudes of the no-load and armature reaction fluxes and the resulting load flux at all positions in Machine A. It is evident that the no-load and armature reaction fluxes are alternately in phase and opposite in phase at every other position. This is the effect of the very high subharmonic content of the stator yoke flux. It is clear that the flux density is not evenly distributed in the back yoke, even over time. The highest flux amplitudes, at positions 3, 7, and 11, are more than four times higher than the flux amplitudes at positions 2, 6, and 10.

The winding configuration of the fractional-slot machine creates an armature reaction flux that does not exhibit the same amplitude behind all slots. In addition, the time-varying armature reaction flux possesses a phase shift with respect to the no-load flux that is not the same behind each slot. Consequently, the flux amplitude differs significantly at different positions.

A single-layer non-overlapping concentrated-coil winding such as that in Machine A produces a large amount of subharmonics. By comparison, the subharmonic content of a double-layer concentrated-coil winding with the same number of poles and slots (Machine B) is significantly reduced [1]. Fig. 15 shows the harmonic contents in the air gap and in the stator back yoke of Machine B. There is no strong subharmonic in the armature reaction field, and the sum of the two flux patterns looks quite different from the single-layer pattern (see Fig. 16). In Machine B, the armature reaction pattern is more variable than that in Machine A, with the highest amplitude being 5.4 times higher than the lowest. This is the phenomenon described in [10]; the armature reaction flux in a machine with double-layer winding and two adjacent teeth wound with the same phase is smaller in some parts of the stator. However, when the armature reaction flux is combined with the no-load flux, the difference between the lowest and highest amplitudes is only 62%.

Machine C is a single-layer distributed winding machine with 1.4 slots per pole per phase. The amplitudes of the no-load, armature reaction, and superposed fluxes are

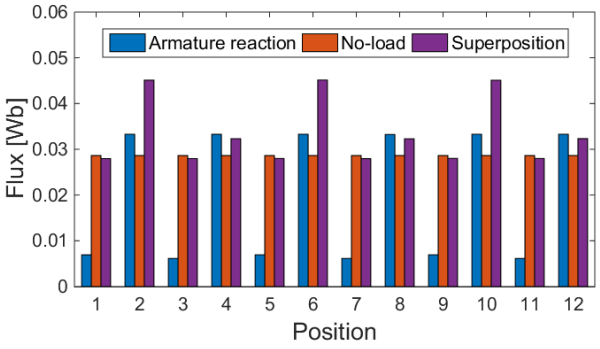

Fig. 16. Machine B: flux amplitudes in positions 1–12.

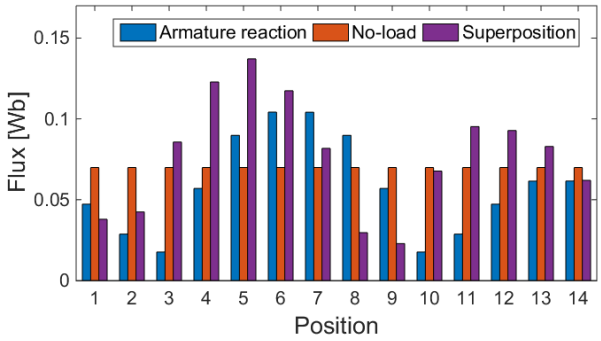

Fig. 17. Machine C: flux amplitudes in positions 1–14.

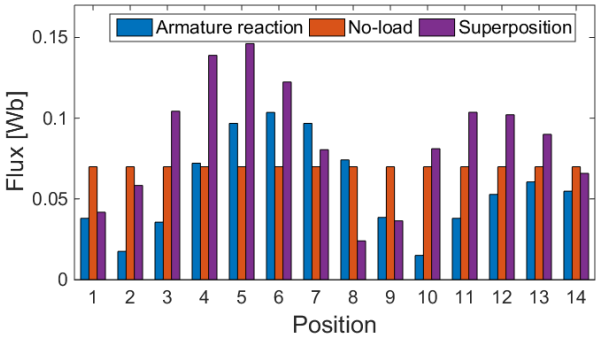

Fig. 18. Machine D: flux amplitudes in positions 1–14.

shown in Fig. 17. It is evident that the flux variation in this machine is also large. The highest flux amplitude is six times higher than the lowest flux amplitude in the case of both the armature reaction flux and the load flux.

Machine D is a double-layer distributed winding machine with the same numbers of slots and poles as Machine C. As seen in Fig. 18, it produces flux patterns similar to those of Machine C, but in the positions with the highest armature reaction flux amplitudes (positions 5–7), the no-load and armature reaction fluxes are more in phase. The maximum amplitude under load is 6.5% higher compared with Machine C, although the highest armature reaction amplitude is slightly lower.

In Table III, the no-load, armature reaction, and superposed fluxes in all four machines are summarized. The top half of the table lists the highest amplitudes observed in the machines,

TABLE III
MAXIMUM AND AVERAGE FLUX AMPLITUDES [mWb] FROM THE ANALYTICAL AND FEA CALCULATIONS

Machine		A	B	C	D
Maximum					
No-load	LPM	28.6	28.6	69.9	69.9
	FEA	28.6	28.6	73.3	73.3
Current reac.	LPM	54.5	33.3	104.2	103.6
	FEA	52.8	40.6	98.5	97.7
Superposed	LPM	82.5	51.4	150.2	146.2
	FEA	80.6	54.7	140.7	152.0
Averaged over all positions					
No-load	LPM	28.6	28.6	69.9	69.9
	FEA	28.4	28.4	73.3	73.2
Current reac.	LPM	50.0	19.9	58.0	56.7
	FEA	47.6	28.1	59.1	57.6
Superposed	LPM	49.9	37.9	87.2	85.4
	FEA	49.4	40.2	82.8	94.3

whereas the bottom half lists the average amplitudes. Numbers from both the FEA simulations and the LPM calculations are included.

IV. DISCUSSION

For machine design purposes, it is important to know the stator flux for two main reasons: to prevent saturation and to calculate iron loss.

In integer-slot machines, no subharmonic flux patterns exist in the yokes, and the armature reaction fluxes are no larger in the yokes than in the air gap. If the air-gap flux is kept relatively low to avoid demagnetization, then the armature reaction does not have a strong impact on the yoke flux magnitude. However, in fractional-slot machines, the combination of the no-load and armature reaction fluxes can lead to yoke fluxes that are much higher than the no-load fluxes. The yoke thickness must be adjusted accordingly if saturation is to be avoided.

It is possible to allow the stator yoke to partially saturate in small sections. This would increase the reluctance in the yoke and act as a flux barrier, reducing the subharmonic fluxes in both the stator and rotor yokes. This is a known method of reducing the induced losses in the rotors of fractional-slot winding machines [16], [17]. Additional flux barriers could also be placed in the locations where the flux is highest. These measures would reduce torque production capability.

The LPM method of calculating the stator yoke flux includes a few simplifications that may cause errors. One is that it assumes a sinusoidal time variation of the fluxes at no-load. This is not necessarily true, especially for machines with many slots per pole.

Iron saturation is not considered. The LPM could be further developed to account for saturation.

The leakage flux model is coarse and could be more detailed for better precision.

Not all slots in double-layer wound machines contain one winding with current distributed evenly in the slots. They will have different leakage reluctances, which also is not taken into account here.

Fig. 19 shows the amplitudes under load in all positions calculated using the LPM and FEA approaches,

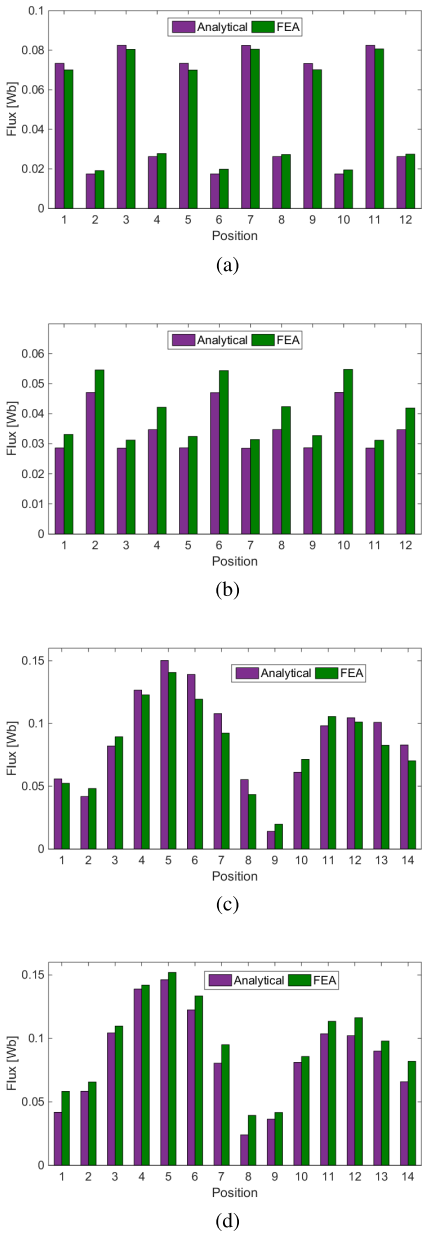

Fig. 19. Superposed amplitudes in Machines A–D. (a) Machine A. (b) Machine B. (c) Machine C. (d) Machine D.

both superpositioned. The analytical model is able to recreate the flux pattern in all machines. The largest error is found in the Machine B calculations. The error lies in the armature reaction flux amplitude and not in the summation of the no-load and armature reaction fluxes. This is likely caused by inexact leakage computations. A quantitative comparison between the analytical and FEA calculations is also presented in Table III. The error in the maximum load flux ranges between 2.3% and 6.1%.

When three phases are symmetrically distributed in one section, the flux pattern is repeated three times within the section. In fractional-slot machines with only three slots per pole ($q = 0.5$), there are only three slots in one symmetrical section; hence, the flux amplitude is the same behind all slots, as was shown in [12].

V. Conclusion

The armature reaction flux should be accounted for in the stator and rotor yokes in a fractional-slot machine, especially when the current loading is high. Although the subharmonic content of the magnetic flux in the air gap can be high, the subharmonic amplitudes in the yokes may be much higher, causing the load flux in the stator yoke to be much higher than the no-load flux.

Two LPMs have been used to determine the no-load and armature-reaction-induced fluxes in such machines. Four different machines have been investigated: two concentrated winding machines and two distributed winding machines, one with single-layer winding and one with double-layer winding of each type. It has been shown that the no-load and armature reaction fluxes combine in different ways in different machines.

The flux amplitudes in the stator yoke are not the same behind every slot of the stator. The winding layout may cause the armature reaction flux amplitude to be distributed unevenly. An even larger variation can occur when the no-load flux and armature reaction flux are combined, because the phase shift between them varies behind different slots. It has been shown that in one of the investigated machines, the load flux amplitude behind one slot is more than six times higher than that behind another slot.

With detailed knowledge of how the magnetic flux is distributed along the stator back yoke, the designer can place the holes for bolts or for cooling in positions that are less saturated. It is also possible to deliberately allow the yoke to saturate in some areas, thereby creating flux barriers and reducing the magnitude of the subharmonic fluxes traversing the machine, potentially reducing rotor losses. Flux barriers designed to reduce the subharmonic fluxes can also be placed in precisely chosen locations when the flux pattern in the stator is known.

Acknowledgment

This work was supported by SmartMotor AS.

References

[1] O. Krøvel, "Design of large permanent magnetized synchronous electric machines," Ph.D. dissertation, Dept. Elect. Power Eng., Norwegian Univ. Sci. Technol., Trondheim, Norway, 2011.

[2] S. Meier, "Theoretical design of surface-mounted permanent magnet motors with field-weakening capability," M.S. thesis, Dept. Elect. Eng., Roy. Inst. Technol., Stockholm, Sweden, 2002.

[3] A. Røkke, "Gradient based optimization of permanent magnet generator design for a tidal turbine," in *Proc. Int. Conf. Elect. Mach. (ICEM)*, Sep. 2014, pp. 1199–1205.

[4] Z. Q. Zhu and D. Howe, "Instantaneous magnetic field distribution in brushless permanent magnet DC motors. II. Armature-reaction field," *IEEE Trans. Magn.*, vol. 29, no. 1, pp. 136–142, Jan. 1993.

[5] E. Fornasiero, "Advanced design of direct drive PM machines," Ph.D. dissertation, Dept. Elect. Eng., Univ. Padua, Padua, Italy, 2010.

[6] C. Mi, G. R. Slemon, and R. Bonert, "Modeling of iron losses of surface-mounted permanent magnet synchronous motors," in *Proc. 36th IAS Annu. Meeting Conf. Rec. IEEE Ind. Appl. Conf.*, vol. 4. Sep./Oct. 2001, pp. 2585–2591.

[7] D. Ishak, Z. Q. Zhu, and D. Howe, "Eddy-current loss in the rotor magnets of permanent-magnet brushless machines having a fractional number of slots per pole," *IEEE Trans. Magn.*, vol. 41, no. 9, pp. 2462–2469, Sep. 2005.

[8] Z. Q. Zhu, K. B. Ng, and D. Howe, "Analytical prediction of stator flux density waveforms and iron losses in brushless DC machines, accounting for load condition," in *Proc. 5th Int. Conf. Elect. Mach. Syst. (ICEMS)*, vol. 2. Aug. 2001, pp. 814–817.
[9] F. Meier and J. Soulard, "Analysis of flux measurements on a PMSM with non-overlapping concentrated windings," in *Proc. IEEE Ind. Appl. Soc. Annu. Meeting*, Oct. 2008, pp. 1–8.
[10] N. Bianchi, S. Bolognani, and M. D. Pre, "Magnetic loading of fractional-slot three-phase PM motors with nonoverlapped coils," *IEEE Trans. Ind. Appl.*, vol. 44, no. 5, pp. 1513–1521, Sep. 2008.
[11] G. Y. Sizov, D. M. Ionel, and N. A. O. Demerdash, "Modeling and design optimization of PM AC machines using computationally efficient—Finite element analysis," in *Proc. IEEE Energy Convers. Congr. Expo. (ECCE)*, Sep. 2010, pp. 578–585.
[12] D. M. Ionel and M. Popescu, "Ultrafast finite-element analysis of brushless PM machines based on space–time transformations," *IEEE Trans. Ind. Appl.*, vol. 47, no. 2, pp. 744–753, Mar./Apr. 2011.
[13] D. C. Hanselman, *Brushless Permanent Magnet Motor Design*. New York, NY, USA: McGraw-Hill, 1994.
[14] H. A. Toliyat and G. B. Kliman, *Handbook of Electric Motors*, vol. 120. Boca Raton, FL, USA: CRC Press, 2004.
[15] P. Salminen, "Fractional slot permanent magnet synchronous motors for low speed applications," Ph.D. dissertation, Dept. Elect. Eng., Acta Univ. Lappeenrantaensis, Lappeenranta, Finland, 2004.
[16] G. Dajaku, W. Xie, and D. Gerling, "Reduction of low space harmonics for the fractional slot concentrated windings using a novel stator design," *IEEE Trans. Magn.*, vol. 50, no. 5, May 2014, Art. no. 8201012.
[17] G. Dajaku and D. Gerling, "Analysis of different PM machines with concentrated windings and flux barriers in stator core," in *Proc. Int. Conf. Elect. Mach. (ICEM)*, Sep. 2014, pp. 375–384.

Astrid Røkke received the M.Sc. degree in electrical engineering from the Norwegian University of Science and Technology, Trondheim, Norway, in 2007, where she is currently pursuing the Ph.D. degree with the Department of Electric Power Engineering.

From 2007 to 2012, she was with SmartMotor AS, where she was involved in the development of permanent magnet machines. His current research interests include modeling and simulation of electrical machines, particularly large permanent magnet machines.

Robert Nilssen received the master's and Ph.D. degrees from the Norwegian University of Science and Technology (NTNU), Trondheim, Norway, in 1983 and 1989, respectively, with a focus on finite-element analysis and electrical machines.

He is currently a Full Professor with the Department of Electrical Power Engineering, NTNU. His current research interests include design, optimization, and modeling of industrial heating products, electrical machines in hydro power, large permanent magnet motors, and generators for various applications, such as ship propulsion, tidal power, floating wind turbines, and axial flux ironless generators, and reciprocating permanent magnet linear machines for high power drilling, vibrator, and compressor applications.

Dr. Nilssen is a Co-Founder of several companies, having successfully turned the university projects into commercial industry companies.